Numerical noise prediction of a generic flap configuration

Lilla Kapa-Koloszar
Patrick Rambaud
Philippe Planquart
Christophe Schram

von Karman Institute
B-1640 Rhode-Saint-Genèse,
Belgium
koloszar@vki.ac.be

Abstract

The present work deals with the turbulent flow simulation of an airfoil with a generic flap. The purpose of this simulation is to provide the time history of the pressure field on the wing and on the flap for noise prediction. The configuration and the flow conditions were defined in the FP7 VALIANT project. Within this framework measurements were performed in Ecole Central de Lyon, to which the present simulation is compared. In order to be able to reproduce the measurements with numerical simulation, the experimental velocity profiles on the middle of the wing were used as inlet boundary conditions. In this work three different inlets were used and the resulting flow fields were compared.

Key words: aerodynamics, large eddy simulation, incompressible flow, high-lift device.

Introduction

During aircraft approach and landing, a significant portion of noise is generated by the high-lift devices. Reducing the noise during landing is very important for the comfort of the residents living nearby an airport. The airframe noise during take-off maneuver is less important, since the slope of the take-off is much steeper, and the engines are in full trust, louder than any other component. Among the various noise sources during approach and landing, the landing gear, leading-edge slat and the side edges of the flap where identified as the main airframe noise sources [2].

In order to isolate the noise produced by an aircraft flap in landing configuration, a semi infinite wing was considered in front of the flap. The flap is placed under the wing with a bit of overlap. This configuration was installed in the anechoic wind tunnel of Ecole Central de Lyon and both flow and acoustic measurements were performed in the framework of VALIANT (VALidation and Improvement of Airframe Noise prediction Tools [3]) FP-7 European project [1]. The main characteristics defining the flow are the free-stream velocity $U_\infty = 51 m/s$, which corresponds to approach condition with $Ma = 0.15$. The resulting Reynolds number, $\mathrm{Re} = 1.36 \cdot 10^6$, is approximately $1/10^{th}$ of the Reynolds numbers corresponds to a real aircraft wing during approach. Roughness elements (sandpaper ISO P150) were placed on both sides of the wing in order to trigger an established incoming turbulent boundary layer. The experimental database obtained by ECL includes the following data: time-dependent microphone signals, time-dependent wall pressure signals, time-dependent series of the velocities acquired from hot wire measurements.

The current paper describes an incompressible Large-Eddy simulation of this geometry with different inlet boundary conditions. The first section describes the computational domain and the structured mesh used. The second part of the paper introduces the numerical method and the boundary conditions applied. The next section

discusses the effect of the inlet boundary condition on the resulted flow field, while the last part concludes the work.

Solution domain and grid

The computational domain and applied boundary conditions are graphically presented in Figure 1. As can be seen in the figure the flap is placed under the wing with a bit of overlap. In the experiments the wing is represented as a semi-infinite plate and it is starting inside the convergence section of the wind tunnel. In the computations half of the semi-infinite wing is considered where hot-wire measurements are available on both side of the wing.

The lateral boundaries are implemented as symmetry planes. The boundary follows the shape of streamlines predicted by the 2D RANS simulation. The downstream boundary is placed 5 flap-chords away from the objects.

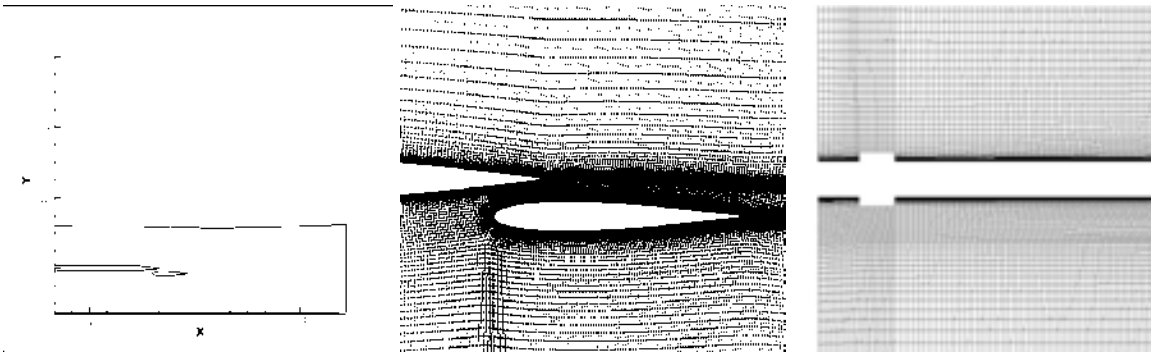

Figure 1: Computational domain, the mesh around the flap and the inlet bump

The grid requirement of high fidelity simulations, such as the presently applied Large Eddy Simulation, is scaling with the Reynolds number on the power of $9/4^{th}$. Therefore, it is still very challenging to perform numerical simulation of a wing with deployed high-lift system due to the high Reynolds number ($Re \sim 10^6$-10^7). This is even truer for acoustic simulations, where the smallest grid size is determined by the Kolmogorov length scale, while the largest grid size is restricted by the frequency resolution of interest.

A block mesh was generated to ensure a mesh with sufficient quality for Finite Volume Method. First, a 2D mesh was constructed and was extruded in the span-wise direction. The measurement setup had quasi-2D geometry as well. The span-wise extend was chosen to be 10% of the setup chord only (chord of the wing + chord of the flap - overlap). The final mesh has 6.08 million cells.

Flap noise is greatly affected by the flow around the main wing. Therefore, a correct representation of the boundary layer on the wing is important. In the present simulation the inflow conditions were provided by hot-wire measurements. In order to capture the dynamics of the incoming boundary layer a dense boundary fitted mesh was generated. The y^+ never exceed 3 in the whole domain.

Aeroacoustic noise at subsonic velocities is mostly generated when turbulent structures impact and pass-over solid boundaries. The overlapping region is highly refined in order to accurately resolve the incoming turbulence arriving from the wing and impacting on the leading edge of the flat. Due to this intensive turbulence-body interaction, the mush weaker noise generated by the finite trailing-edge is neglected. A sharp trailing edge was considered in case of the wing and in case of the flap as well.

Away from the region of interest, the grid was coarsened in order to keep to the minimum the cost of the computation. Previous studied showed that the grid can induce spurious reflections if the cell-to-cell ratio is higher than 1.1, so the grid coarsening was performed according.

Model and simulation details

The setup described in the previous section is initialized by a steady-state RANS simulation. Then the incompressible Large-Eddy simulation solver of the open-source simulation environment OpenFOAM version 1.7.1 [4] was used in order to resolve the pressure fluctuations in time on the solid surfaces. The dynamic Smagorinsky model was used to model the unresolved scales.

In the first part of the unsteady simulation a first order upwind scheme was used (half flow through) and once the flow was established it was changed to second order upwind combined with backward Euler time discretization. The time-step was chosen to keep the Courant number under 0.75. Accumulation of data for averaging purposes only commences after flushing of the calculation domain for three and a half flow-through time. Ideally the averaging time should be large enough so that the mean data reaches steady state. Computations were carried out on the SGI Altix ICE 8200 dual plane cluster of VKI (64 blades equipped with 128 quad cores Xeon processors at 2.5 Ghz/12M/1333MHz, with 256 set of 4 GB DIMM (2x2GB 667 MHz) and Infiniband connection). 0.001s of simulation time took approximately 30 CPU hours of physical time on 64 nodes.

In the measurements, at the inlet of the wing, a turbulent strip was attached to in order to mimic the flow field induced by a deployed slat. Three different approaches have been used to impose the inlet boundary condition in the numerical simulation. In all the cases, the measured, time-averaged velocity profiles were used as base. In Case 1 no perturbations were imposed to this profile, in Case 2 random perturbations were superimposed, which were scaled with the measured turbulent intensity. This approach is rather rough, since turbulence is much more than a random perturbation around the mean flow. The coherence of the incoming boundary layer won't be captured that way, but it was hoped that the long wing section will be enough to build up the missing coherence.

Finally, in Case 3, again a constant profile was used, but the wing geometry was modified such that the turbulent strip was represented by a bump. As it can be seen in the right side of Figure 1, the mesh is not resolved around the bump, since the aim of the object is only enhance turbulence and not its correct physical description. The height of the bump was chosen to 5mm, which is approximately half of the boundary layer thickness on the wing. This height is somewhat arbitrary and needs further investigation to correlate it with the desired r.m.s. velocity.

The three different boundary conditions are summarized in Table 1.

Table 1: Simulation cases

Case specification	***Applied inlet boundary condition***
Case 1	Mean velocity profiles
Case 2	Mean velocity profiles with random perturbation
Case 3	Mean velocity profiles with bump

Above and below the wing, the free-field boundaries were set as symmetry planes. These boundaries were extracted along the streamlines of an initial 2D RANS simulation of the whole experimental setup, through which no flow is possible. On the spanwise boundaries periodic boundary condition is applied, since it was not possible to simulate the whole experimental domain with the endplates due to the high computational cost. Measurements later confirmed that the shielding of the endplates successfully reduced the noise generated by the flow around them, so considering just this small slice of wing with periodic BCs can be sufficient [3].

Flow features and dynamics

Case 1 and Case 2 gave approximately the same velocity filed, so in the following Case 1 and Case 3 will be compared. The first set of results show the flow around the wing and flap in a pure qualitative sense. The different inlet approaches results in different flow fields. The suction side of the main wing is undisturbed. In Case 1 and 2 a recirculation zone is formed near the trailing edge upstream. At the pressure side the recirculation bubble is still present, but its size is smaller than on the suction side, due to the accelerated flow between the wing and flap (Figure 2). Three separation bubbles are predicted by Case 1 (and 2) simulation.

There is one large in the upper part of the wing around the trailing edge and one smaller in the lower part. The third separation bubble can be found at the lower part of the flap trailing edge.

.

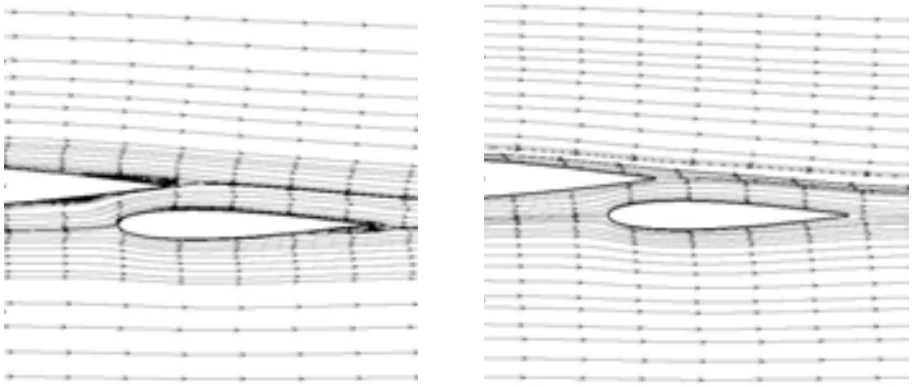

Figure 2: Mid-span plane velocity: mean streaklines: Case 1 (left) and Case 3 (right)

In the simulation with the bump no separation bubble is present. This is due to the higher energy contents of the turbulent boundary layer triggered by the bump. The flow is indeed turbulent over the wing as visualized by the Q structures in Figure 3. In case of the random perturbations no coherent structures can be observed over and below the wing, transition to turbulence starts at the wing trailing edge. In order to trigger the turbulence along the wing, the magnitude of the random perturbation was increased, but this attempt leaded the simulation to diverge.

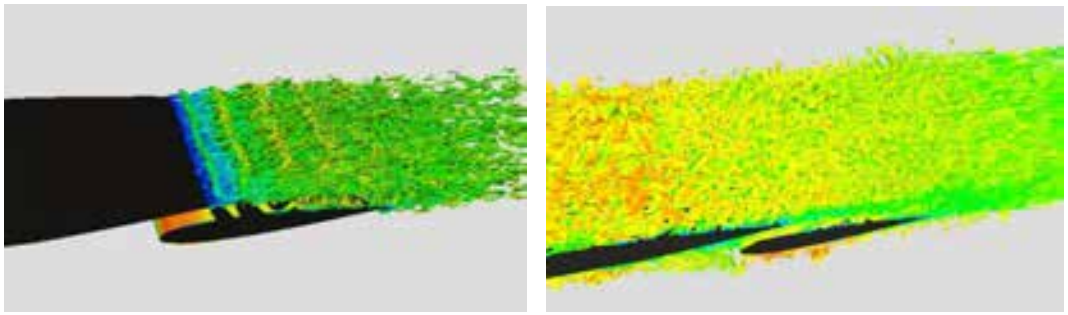

Figure 3: Iso-Q surfaces colored by the velocity magnitude (Q=106). Left – Case 1, right – Case 3

It can be seen (Figure 4) that in Case 1 periodic vortices are shedding from the main wing trailing edge. These vortices partially impact on the flap suction side. The presence of the strong vortex shedding is the indication that the boundary layer on the wing stays laminar. These structures travel along the flap and are feeding energy into its boundary layer, such that it stays attached. The strong periodic vortices are not present in the Case 3 simulation. Much weaker, but more distributed velocity fluctuations can be observed in the right side of Figure 4, corresponding to this simulation.

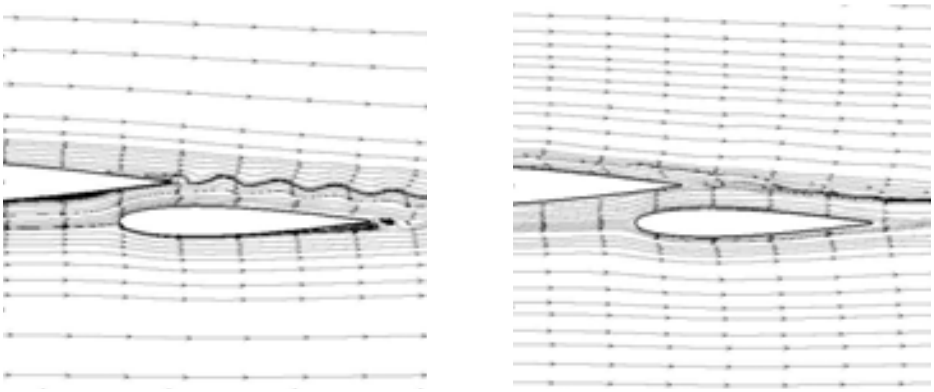

Figure 4: Mid-span plane velocity: instantaneous streaklines: Case 1 (left) and Case 3 (right)

Indeed, in Figure 5 we can see that the vorticity is homogenous along the wing in Case 1, while shows a turbulent structure for Case 3. On the left figure, strong large vortices can be identified, while on the right figure several, small fluctuations are visible.

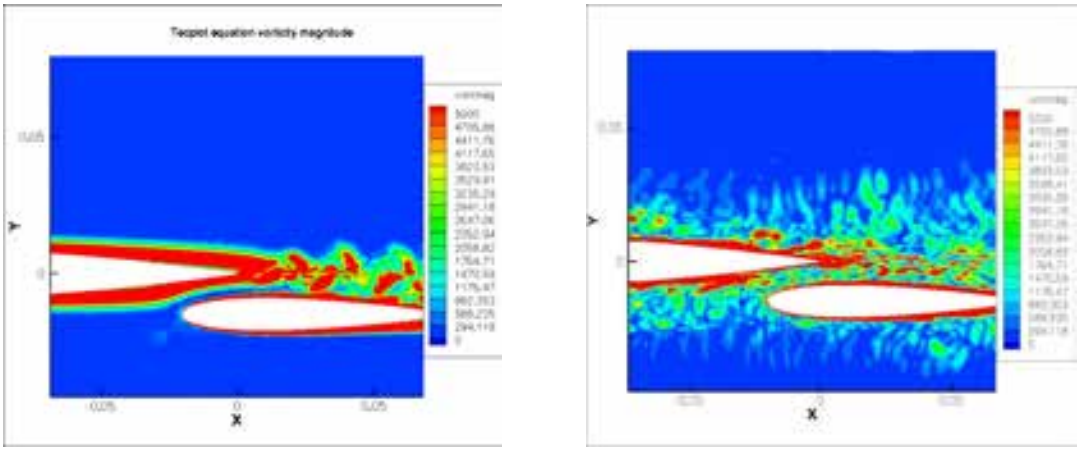

Figure 5: Mid-span instantaneous vorticity at the mid-plane: Case 1 (left) and Case 3 (right)

Figure 6 and Figure 7 compares mean- and r.m.s. velocity profiles at two streamwise locations. The first velocity profile is extracted *5mm* upstream to the wing trailing edge. It means that it contains the boundary layer of the wing suction side, the gap between the wing and the flap and the boundary layer on the flap pressure side. As we can see on the mean velocity profiles, the application of the bump indeed improves the boundary layer on the wing, however we got a faster flow along the flap and inside the gap, than in case of the laminar inflow. Moving downstream on the flap, the situation improves a bit on the suction side of the flap, however, the CFD simulation still over predicts the experimental values.

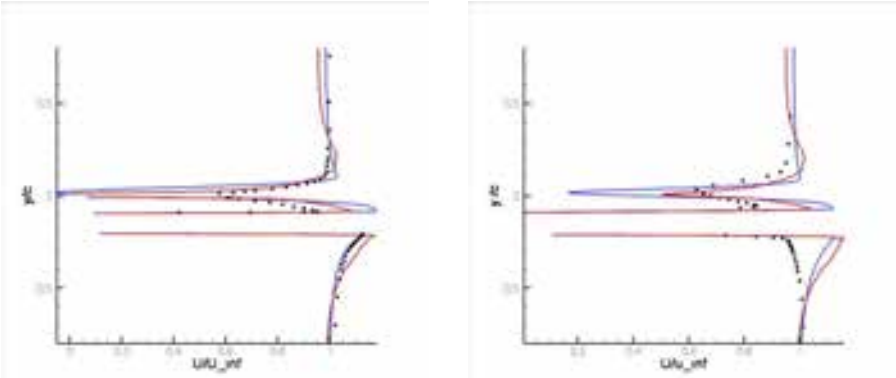

Figure 6: Mean streamwise velocity profiles 5mm before the wing trailing edge and before the flap trailing edge (x= -0.005, 0.079). Black dots – measurement, blue line – Case 1, red line – Case 3.

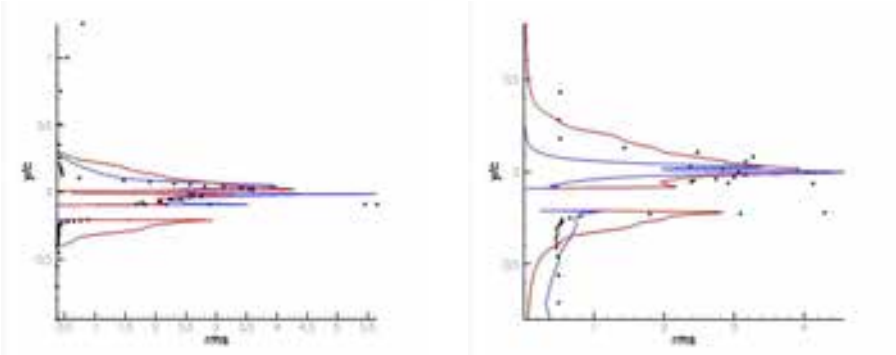

Figure 7: R.m.s. streamwise velocity profiles at 5mm before the wing trailing edge and before the flap trailing edge (x= -0.005, 0.079). Black dots – measurement, blue line – Case 1, red line – Case 3.

The wall pressure sensors in the experiments are indicated in Figure 8.

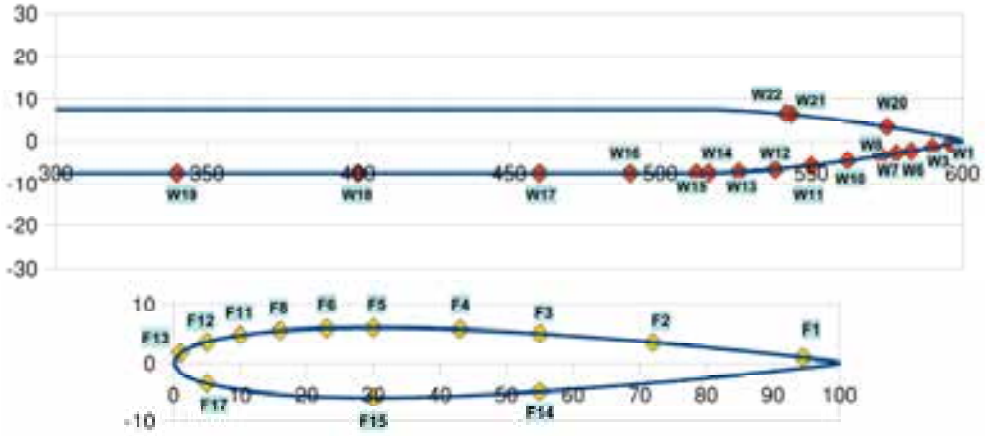

Figure 8: Wall pressure sensors along the wing and the flap

After post-processing the wall-pressure signals at different locations another artefact of the random turbulent inlet were discovered. Despite the laminar, but still meaningful velocity field, the pressure signal was completely uncorrelated due to the white noise inlet perturbation (Figure 9).

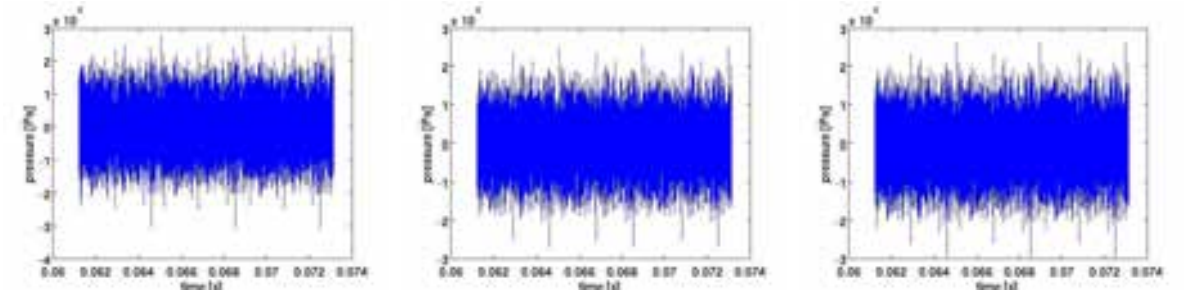

Figure 9: Case 2 pressure time-history at various x locations (W12, W15, W20)

To cure this problem, the random perturbation at the inlet has been switched off. Within few time-steps, the pressure signal seemed to be recovered (Figure 10).

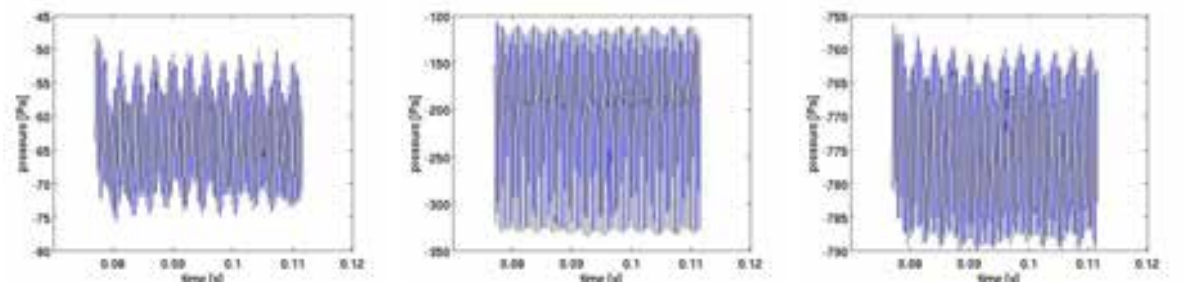

Figure 10: Case 1 pressure time-history at various x locations (W12, W15, W20)

Turning off the random velocity perturbation gave a correlated velocity-pressure signal, but is resulted a laminar dominated flow-field. To be able to reproduce the physics in the experiments a physical bump was introduced in the solution domain mimicking the effect of the turbulent strip. As we could see previously, the flow structure around the wing and flap has changed considerably. The mean and r.m.s. velocities got closer to the measured ones. The corresponding pressure signals are less periodic than the ones correspond to the laminar Case 1 simulation (Figure 11). The simulation time corresponding to Case 3 is approximately half of the other two, which means that we should expect less accurate pressure spectra in the low frequency range corresponding to this case.

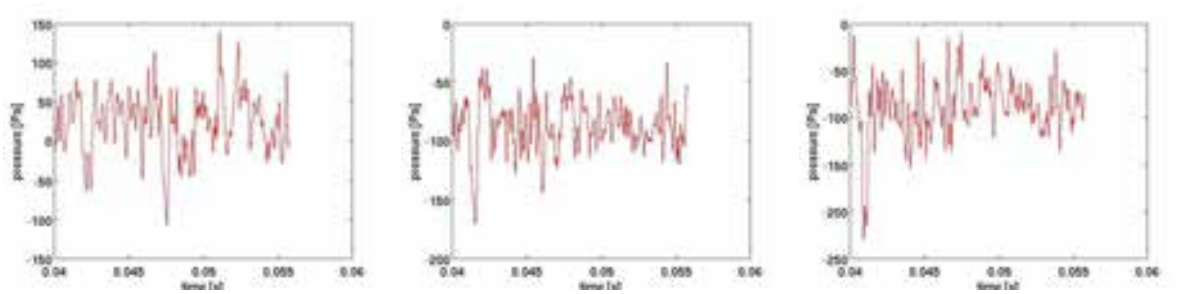

Figure 11: Case 3 pressure time-history at various x locations (W12, W15, W20)

In the following, the wall pressure spectra of Case 1 and Case 3 will be compared with the measurement data provided by ECL in various locations. Figure 12 shows three pressure spectra on the wing. The first probe depicted is located on the pressure side furthest upstream from the wing trailing edge. The measurement shows a completely broadband spectrum, indicating an energetic, stable turbulent boundary layer. At the high frequency region ($f \approx 9-10kHz$) there is a tonal peak which can be found in the next spectra corresponding a bit further downstream, but on the suction side. They are both very close to the geometrical change due to the trailing edge, which might induce some high frequency instabilities. This effect cannot be observed any more very close to the trailing edge, Figure 12 last picture, where the spectrum is decaying in the high frequency region. This high frequency bump is not reproduced by any of the simulations due to the insufficient grid resolution.

The laminar-like vortex shedding is pronounced by a strong peak in the pressure spectra corresponding to Case 1. The vortex shedding frequency is 1100 Hz. This peak can be observed in all the spectra due to the non-compactness of the trailing edge noise. In the Case 1, all other frequencies are damped and the general broadband noise level is lower.

The turbulent boundary layer corresponding to Case 3 results in a completely broadband spectrum, all the frequencies represented equally. This simulation is capturing better the measurements. The discrepancies in the low frequencies are due to the short simulation time, as pointed out earlier.

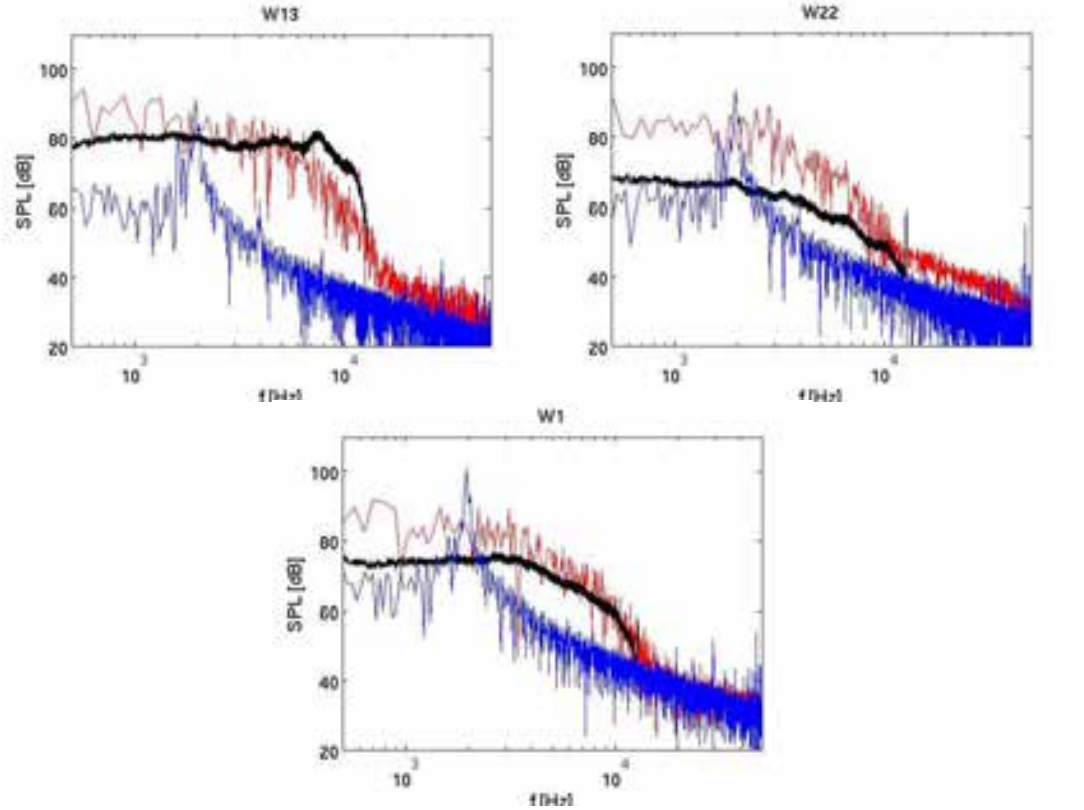

Figure 12: Pressure spectra on the wing. Black – measurements, blue – Case 1, red – Case 3.

Figure 13 shows pressure spectra on the flap starting from the flap trailing edge suction side to the leading edge till the flap pressure side trailing edge. Along the suction side in the laminar case, Case 1, not just the main vortex shedding frequency is present, but its harmonics, too, indicating vortex pairing along the passage over the flap. In pressure spectra corresponding to the pressure side only the vortex shedding peak is present. Again, the Case 3 simulation compares better with the measurements. However, it over predicts the measured noise levels close to the leading edge of the flap, which means that the incoming boundary layer is more energetic in the simulation than in the experiments. This is confirmed by the higher r.m.s. velocity levels shown in Figure 7.

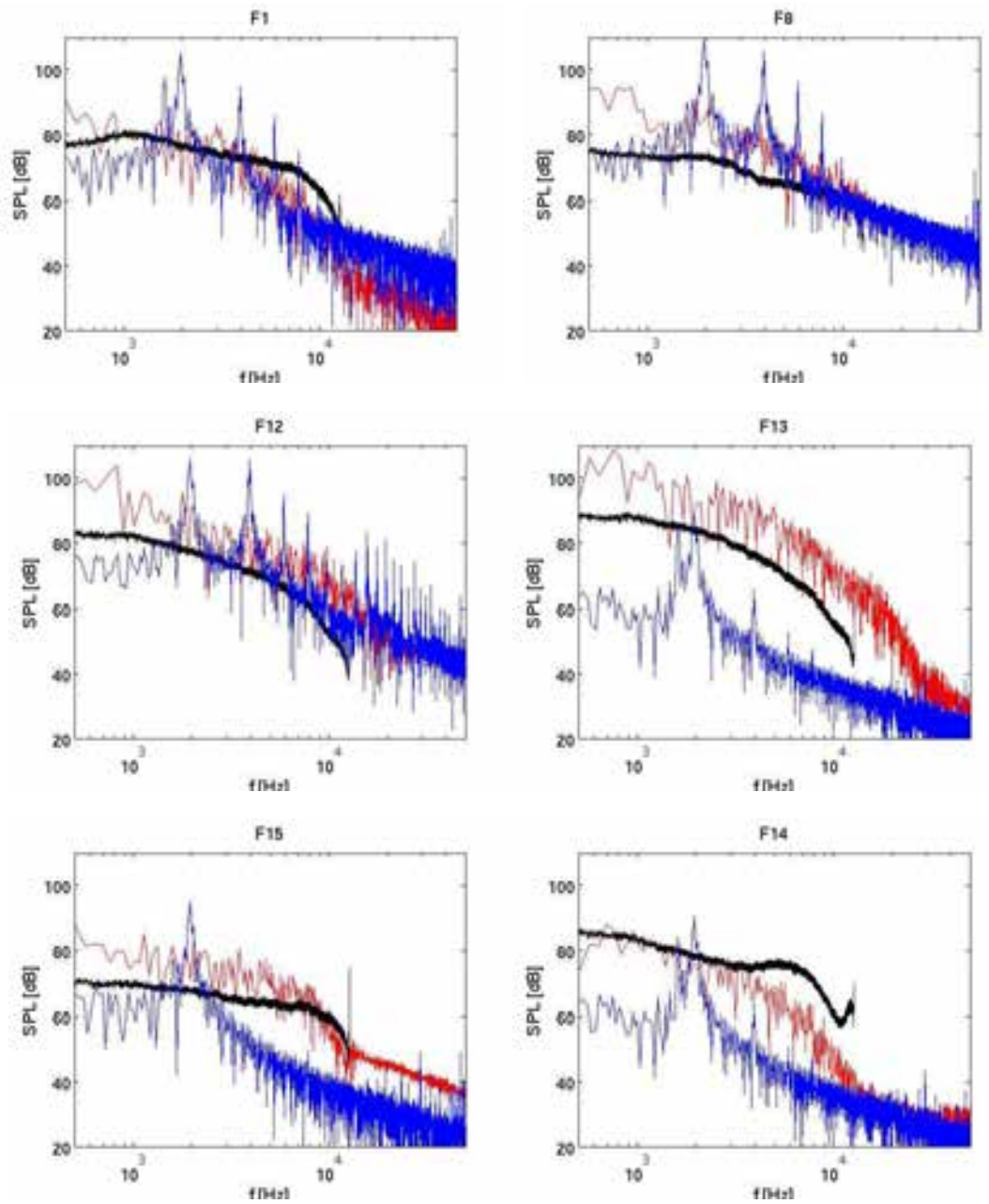

Figure 13: Pressure spectra on the flap. Black – measurements, blue – Case 1, red – Case 3.

The spectrum at the trailing edge of the flap is very similar to the ones on the wing. The shape is different, however, in the flap nose region. The turbulence arriving from the wing impinges to the flap inducing higher noise levels in the low frequency regions, while lower levels in the high frequency region. This is most probably due to the fact that in the leading edge region the turbulent boundary layer is not developed yet. A relatively homogeneous turbulence is impinging on the flap, which gives the decaying spectrum. At the suction side, the

decay is less fast. Due to the gap, the structures got elongated which feeds energy to the mid-frequency region. These elongated structures then interact with the shear layer developed after the wing trailing edge and are advected downward along the flap suction side.

Conclusions and further work

An incompressible Large-Eddy Simulation was carried out to study the aerodynamics of simplified flap and wing configuration, with a particular emphasis on the pressure field on the solid surfaces. Three different inlet boundary conditions were used in order to reproduce the measurements performed at Ecole Central de Lyon. This comparison showed that the inlet boundary condition strongly determines the physics involved in the numerical simulation. Imposing a steady measured profile at the inlet of the computational domain resulted in a laminar vortex shedding from the wing trailing edge. This deterministic behavior is not present in the measurements. Therefore, a better representation of the flow field in the experiments thought to be achieved by triggering the incoming flow.

Two simple approaches were used to establish a turbulent boundary layer over the wing. First a random perturbation was superimposed to the mean measured velocity profile. Since it resulted in an uncorrelated pressure field a different solution had to be found. A physical bump was added to the computational domain to mimic the strip installed on the wing in the experimental mock-up. The effect of the bump was not strongly pronounced in the mean and r.m.s. velocity profiles, but are well visible in the vorticity field. The flow turned to turbulent over the wing, as desired. It has improved significantly the pressure spectra indicating that the energy contents of the flow have changed due to the presence of the bump in the right direction.

None of the simulations were able to reproduce the high frequency peak in the pressure spectra close to the wing or the flap trailing edge due to the insufficient grid resolution. Besides this, the Case 3 simulation fairly well captures the spectra along the wing. The spectrum at the trailing edge region of the flap is very similar to the ones on the wing and the pressure levels are well captured by this simulation, too. In the flap leading edge region the spectra is considerably different. It resembles more to the spectrum corresponding to homogeneous turbulence. Indeed, the upper part of the wing boundary layer is impinging to the flap nose, where the boundary layer is not developed yet. In terms of pressure levels, this is the region where most deviation is observed, indicating that the turbulence level of the wing boundary layer is higher than the one present in the measurements.

The current simulation successfully reproduces the basic physics that occurs in the generic wing with flap configuration, however some improvements are still recommended. The mesh should be refined in the wing and flap trailing edge region in order to capture the high frequency peak in the spectra. The height of the bump added to the computational domain should be optimized to retrieve the correct dynamics of the boundary layer along the wing.

Acknowledgement

This research is supported through the European FP7 Project VALIANT (contract no AGCP8-GA-2009-233680). The authors are very grateful to B. Lemoine and M. Roger from ECL for providing the measurement data. Special thanks to Michael Shur (NTS), Thilo Knacke (TUB) and M. Terracol (ONERA) for the fruitful discussions.

References

[1] B. Lemoine, M. Roger & I. Legriffon: Aeroacoustics of a Model Non-Lifting Wing-Flap System in a Parallel Flow, 17th AIAA/CEAS Aeroacoustics Conference, 6-8 June, Portland OR, AIAA paper 2011-2735, 2011.

[2] W. Dobrzynski, K. Nagakura, B. Gehlar and A. Buschbaum: Airframe noise studies on wings with deployed high-lift devices, AIAA - 98-2337, 1998

[3] http://www.cimne.com/websasp/valiant/

[4] http://www.openfoam.com